Competitive Adsorption Processes at Clay Mineral Surfaces: A Coupled Experimental and Modeling Approach

Esra Orucoglu, Sylvain Grangeon, Alexandre Gloter, Jean-Charles Robinet, Benoît Madé, Christophe Tournassat

ACS EARTH AND SPACE CHEMISTRY

http://pubs.acs.org/journal/aesccq

Article

Competitive Adsorption Processes at Clay Mineral Surfaces: A Coupled Experimental and Modeling Approach

Esra Orucoglu,* Sylvain Grangeon, Alexandre Gloter, Jean-Charles Robinet, Benoît Madé, and Christophe Tournassat

Cite This: *ACS Earth Space Chem.* 2022, 6, 144−159

Read Online

ACCESS | Metrics & More | Article Recommendations | Supporting Information

ABSTRACT: Quantification of adsorption processes on clay mineral surfaces is often necessary to predict the extent and the evolution of contaminants' migration in surficial and underground environments. Many studies have been dedicated to retention measurement as a function of pH and ionic strength in relation with the two main identified adsorption processes for clay minerals, that is, cation exchange on their basal surfaces and surface complexation on their edge surfaces. The latest process has been repeatedly assessed as an effective retention mechanism at circumneutral pH conditions, which often prevail in natural environments. This assessment must however be tempered by the lack of information about competitive processes that can take place with the numerous chemical species present in natural settings, compared to simplified systems investigated in laboratory experiments. In this study, we quantified experimentally the competition between Pb^{2+}, Co^{2+}, Zn^{2+}, and Mg^{2+} for specific adsorption on montmorillonite edge surfaces. Zn^{2+} was an effective competitor with Pb^{2+} and Co^{2+}, and our results showed also unambiguously the influence of Mg^{2+} concentration levels on the specific adsorption of Pb^{2+} and Co^{2+}. Because of the high ionic strength used in the experiments, cation exchange with Mg^{2+} was dismissed as a possible reason for such competition process, leaving specific competitive adsorption on edge surfaces as a unique explanation for our observations. Modeling of Pb^{2+} adsorption data with a state-of-art electrostatic complexation model for montmorillonite edge surfaces, supported by state-of-the-art, made it possible to distinguish two types of possible competition driving forces: Zn^{2+} competition for adsorption site occupancy but also detrimental changes in surface electrostatic potential following Mg^{2+} adsorption on sites neighboring those of Pb^{2+} adsorption. Mg^{2+} competition observed in our experiment should apply in most of clayey environments. Consequently, adsorption data obtained on pure clay mineral phases, and the associated models that have been built based on these data without considering the geochemical background in competitive species, may overestimate the retention properties of clay minerals when applied to natural settings.

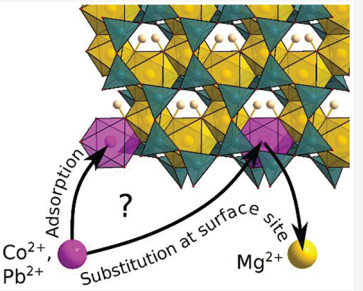

KEYWORDS: *Adsorption, Competition, Surface complexation modeling, Clay, Montmorillonite*

1. INTRODUCTION

Harmful effects to the living by metal and metalloids (hereafter referred as "metals) arise from both natural and anthropogenic sources.[1−5] Because metals are non-degradable, they are prone to bioaccumulation in the food chain and, depending on their speciation, to causing serious disorders to the biota, including human beings.[2,6,7] For these reasons, the mobility and bioavailability of metals in soils, sediments and host rocks for waste disposal sites have been extensively studied in the last few decades.[8−10] A large part of these studies have been focused on the mechanisms by which metals are immobilized on the solid phase, such as adsorption processes, which helps to mitigate toxicological and radiological hazard by limiting metals mobility and availability in aqueous solution.[11,12]

In surficial environments, humic and fulvic acids, iron and manganese oxides, and clay minerals are usually recognized as the main contributors to the retention of metals and radionuclides.[3,8,13−18] Among all reactive phases, clay minerals are certainly most abundant in many soils, sediments, and sedimentary rocks. They are also important components in waste confinement materials.[19−21] Adsorption properties of smectites, which are among the most abundant clay minerals, are related to their structural characteristics: first, a large specific surface area and of a permanent negative layer charge that provide them with large cation exchange capacities; and second, the presence of reactive hydroxyl groups at their edge surfaces, which can bind specifically a range of chemical species.[22−26] Several factors influence the retention of metals on clay mineral surfaces (Figure 1). The effects of pH, ionic strength, and the nature of the background electrolyte, on the nature and extent of the main retention mechanism have been reported on purified and raw clay materials.[22,26−28] At low pH, adsorption is dominated by cation exchange processes on basal

Received: September 20, 2021
Revised: December 17, 2021
Accepted: December 20, 2021
Published: January 5, 2022

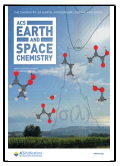

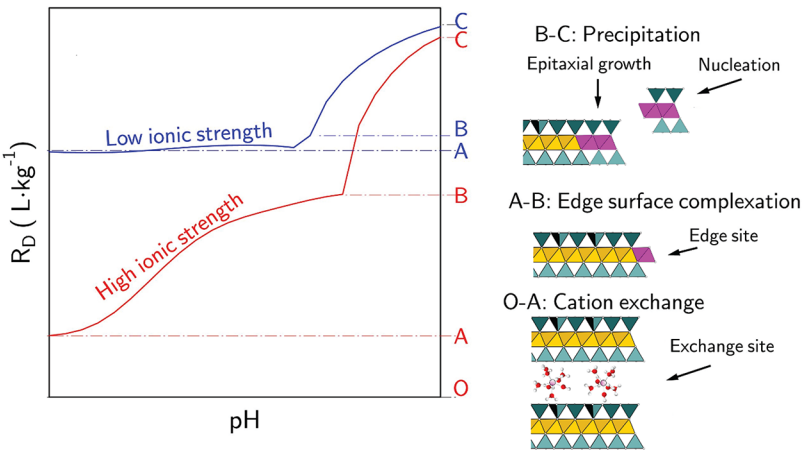

Figure 1. Sorption processes as a function of pH and ionic strength. Dominant mechanisms are cation exchange between O and A region, edge surface complexation between A and B region and precipitation between B and C region.

surfaces (Figure 1). In contrast, at pH values close to neutrality or higher, adsorption is dominated by surface complexation reactions on edge surfaces (Figure 1). Correspondingly, the value of ionic strength has a large influence on the adsorption extent at low pH, while it has a limited influence at high pH.[29−31] Since adsorption is a competitive process, variations in aqueous solution ionic composition may affect the retention of species of interest. Unfortunately, most of previous studies reported only the concentration of the (adsorbed) investigated element at given ionic strength and pH, without additional information on the aqueous solution composition.[27,32−35] Bradbury and Baeyens[28] drew attention to the importance of quantification of background cationic species in the adsorption experiments, which could help to model adsorption data and to understand the system properly. They revealed that impurities could have significant influence on potentiometric titration results and on adsorption measurements, not only in the conditions in which cation exchange dominates, but also in conditions in which specific adsorption through surface complexation on edge surfaces prevail. Serrano et al.[12] emphasized that single ion adsorption investigations can be used for the prediction of adsorption of species that have the strongest adsorption affinity but that they most likely overestimate the adsorption of species of lesser affinity because of competition processes.

In the past decade, competitive adsorption processes on clay minerals attracted more attention.[5,24,36−40] The observation of competition effects were however often limited to conditions for which cation exchange processes are dominant,[5,36] or to conditions in which metals or radionuclides at relatively high concentration compete for adsorption sites.[37,38,40] In clay rock pore water, it has been proposed that some elements present at low concentration such as Zn^{2+} can become effective competitors for adsorption on edge surface sites[30,41] and can be consequently detrimental to radionuclide adsorption. In contrast to elements present at low concentration, the influence of main solution ions, especially cations (Na^+, K^+, Ca^{2+}, Mg^{2+}), on adsorption processes in natural waters, has been relegated systematically to the role of competitors for cation exchange sites only. While this hypothesis is certainly justified for Na^+ and K^+, the case of Mg^{2+} is debatable, because of its high abundance in the clay minerals octahedral layer, which may warrant a specific affinity of Mg^{2+} for the local structural environment that is present at clay mineral edge surface sites.

The objective of the present contribution was to quantify the competition effects between metallic ions as well as between metallic ions and Mg^{2+} and to explore how current state-of-the-art adsorption modeling concepts developed for clay minerals can reproduce these competition effects. We focused our efforts on adsorption of Pb^{2+} and Co^{2+}, which are common metals released from activities like mining, smelting, fossil fuel combustion, refining, manufacturing, and metal recycling.[42−44] Pb^{2+} and Co^{2+} were also chosen because they provide, respectively, contrasted strong and weak adsorption behavior on clay edge mineral surfaces.[30,41] We assigned the role of competitors to Zn^{2+} and Mg^{2+} because of their ubiquity in the environment. The tested modeling approach was the electrostatic surface complexation model we developed recently for montmorillonite edge surfaces[45,46] and that was applied to data we collected specifically for this study as well as literature data. In this model, as in many other surface complexation models, it is assumed that elements are adsorbed at specific crystallographic sites to which are assigned given acidity constants and a given affinity for the elements of interest. Consequently, a strong underlying hypothesis is that the edges have crystalline structure and that the layer charge is homogeneous, that is, that the layer structure is homogeneous, for example, with regards to the cis-vacant or trans-vacant character.[45,47,48] This was tested for our clay sample using high-resolution scanning transmission electron microscopy.

2. THEORETICAL BACKGROUND

Edge surfaces of clay minerals in general, and montmorillonite in particular, have unique electrostatic potential characteristics, which are not similar to electrostatic potentials at simple oxide surfaces.[30,45,46,49] In aqueous dispersion, because of the large aspect ratio of montmorillonite layers and of the presence of a permanent basal surface charge the edge surface potential is affected from charge density at both edge and basal surfaces depending on ionic strength and on the number of stacked layer in a single particle. The influence of the basal surface charge on the edge surface potential is named the spillover effect.[50] The spillover effect has a significant influence on the adsorption properties of clay edge surfaces because it influences the charge-electrostatic potential relationship that

https://doi.org/10.1021/acsearthspacechem.1c00323
ACS Earth Space Chem. 2022, 6, 144−159

Table 1. Summary of Conditions for Time Dependent Adsorption/Desorption Experiments

	step 1 - initial condition				step 2 - adsorption		step 3 - competition	
experiment	R_{sl} (G·L^{-1})	Ph	NaCl (Mol·L^{-1})	Mg^{2+} (Mmol·L^{-1})	Pb^{2+}/or Co^{2+} (Mmol·L^{-1})		Mg^{2+} (Mmol·L^{-1})	Zn^{2+} (Mmol·L^{-1})
K1a	10.2	6.9	0.3		Pb^{2+}	11.4	9.4	
K1b	10.1	7.0	0.3		Pb^{2+}	10.0	6.9	
K2	10.0	6.9	0.3	9.8	Pb^{2+}	11.4		145
K3	10.1	6.9	0.3		Co^{2+}	12.0	11.1	
K4	10.1	6.9	0.3	10.6	Co^{2+}	11.8		118

controls the electrostatic contribution to the adsorption driving forces.[30,45,46,49,51−53]

In an attempt to take into account this specificity of clay mineral edge surfaces, Tournassat et al.[45] developed a generic surface complexation model (SCM) for montmorillonite edge surfaces perpendicular to [010] and [110] and quantified the acid base chemistry of montmorillonite. They defined five possible edge surface functional groups formed by two tetrahedral (labeled T) and one octahedral (labeled Oc) cation with their associated OH groups: Si_T-Al_{Oc}-SiT (labeled S_aOH), Si_T-Mg_{Oc}-Si_T (labeled S_bOH), Al_T-Al_{Oc}-Si_T (labeled S_cOH), Si_T-Fe^{II}_{Oc}-Si_T (labeled S_dOH), and Si_T-Fe^{III}_{Oc}-Si_T (labeled S_eOH). Acid−base properties of these functional groups were obtained from first principle molecular dynamics studies conducted by Liu and co-workers.[54−56] Site densities were calculated from a clay unit cell formula. Electrostatic potential at edge surfaces (ψ_{edge}) were calculated by using the following formula derived from the output of a two-dimensional Poisson−Boltzmann model[30,45,49]

$$\frac{F\psi_{edge}}{RT} = A_1 \operatorname{asinh}(A_2(Q_{edge} + A_3)) \quad (1)$$

where F is the Faraday constant (96 485 C·mol^{-1}), R is the ideal gas constant (8.314 J·mol^{-1}· K^{-1}), T is temperature (in K), Q_{edge} is the surface charge at the edge (in C·m^{-2}), A_1, A_2, and A_3 are parameters obtained from the fit of the two-dimensional Poisson−Boltzmann calculation. A_1 = 1.4−1.2 log I, A_2 = 11 + log I, and A_3= −0.02 × (−log I)$^{1.60}$ where I is the ionic strength (unitless). This surface complexation model offers the advantage to take into account the specificity of the surface charge−electrostatic potential relationship of clay minerals as well as the recent progress made in the prediction of surface site reactivity using theoretical atomistic calculation methods. It was successfully applied to model U(VI) adsorption onto montmorillonite surfaces in a range of chemical conditions.[46,53] Nonetheless, several hypotheses underlying this model must be verified, and its predictive capabilities must be tested further against additional data with increasing complexity. The crystallographic orientation of the edge surfaces and the existence of various functional groups on these surfaces are fundamental assumptions of the model. Theoretical calculations predicted that the most abundant edges surfaces are perpendicular to [010] and [110] crystallographic directions.[57−59] This preferred orientation was evidenced recently by direct observations using AFM techniques.[60] The crystalline nature of clay mineral edge surfaces is another prerequisite to the applicability of the model that builds on an edge surface structure that is identical to the structure of the inner layer. This crystalline nature of edge surfaces can be tested directly by imaging clay mineral layer with atom−resolution techniques. The possible competition of Mg^{2+} with other adsorbates on edge surface adsorption processes can also be viewed as an indirect test of this assumption. By testing the crystalline edge surface assumption with a direct and an indirect approach, the present study provides the necessary materials to a build further mechanistic understanding of clay edge surface−adsorbates interactions.

3. MATERIAL AND METHODS

3.1. Chemicals and Clay Materials. All chemicals used in the experiments were of analytical grade: $Pb(NO_3)_2$ (Prolabo R.P. Normapur, >99.5%), $Co(NO_3)_2{\cdot}6H_2O$ (Merck, >99%), $Zn(NO_3)_2{\cdot}6H_2O$ (Merck, >98.5%), $MgCl_2$ (Merck, >99%), NaCl (Prolabo, 98%), 30% HCl (Merck, Suprapur), NaOH pellets (Prolabo Rectapur >97%), 65% HNO_3 (VWR Prolabo, 69.4%), and MOPS ($C_7H_{15}NO_4S$, Acros Organics, 99%). Ultrapure water (Milli-Q, resistivity = 18 MΩ·cm) was used in all solution preparation and clay dispersion. Kunipia-P and Kunipia-F are industrial products from Kunimine Industries Co. Ltd. that contain 99% and 97% montmorillonite, respectively.[61,62]

3.2. Concentration and pH Measurements. pH measurements were conducted before each sampling event using a digital pH meter (WTW pH 197) and a pH electrode immersed in the glass reactor of kinetic experiments and into the tubes before centrifugation in batch experiments. Pb^{2+}, Co^{2+}, and Zn^{2+} concentrations were measured by inductively coupled-plasma mass spectrometry (ICP-MS-NEXION 350 X, PerkinElmer). Mg^{2+} concentrations were measured using flame atomic absorption spectroscopy (Varian SpectrAA-220 FS).

3.3. Quantification of Adsorption. Adsorption percentages (% adsorption, dimensionless) and distribution coefficients (R_D in L·kg^{-1}) were calculated from the initial added concentration (C_{init} in mol·L^{-1}), the equilibrium measured concentration (C_{eq} in mol·L^{-1}), and the solid concentration (R_{SL} in kg·L^{-1}).

$$\%\text{adsorption} = 100 \times \frac{C_{init} - C_{eq}}{C_{init}} \quad (2)$$

$$R_D = \frac{C_{init} - C_{eq}}{C_{eq} \times R_{SL}} \quad (3)$$

The R_D error bands, ΔR_D, were calculated as follows[30]

$$uR_D = \sqrt{\left(\frac{uC_{tot}}{R_{SL}\cdot C_{eq}}\right)^2 + \left(\frac{C_{tot}\cdot uC_{eq}}{R_{SL}\cdot C_{eq}^{\,2}}\right)^2} \quad (4)$$

$$\Delta R_D = k \times R_D \quad (5)$$

where k was the coverage factor (taken at a value of k = 2), and uC_{tot} and uC_{eq} were the uncertainties associated with the total concentration and the equilibrium concentration respectively

https://doi.org/10.1021/acsearthspacechem.1c00323
ACS Earth Space Chem. 2022, 6, 144−159

Table 2. Summary of Conditions for Pb^{2+} Batch Adsorption Tests

experiment	$[Pb^{2+}]_{init}$ (μmol·L^{-1})	$[Mg^{2+}]_{init}$ (mmol·L^{-1})	$[Zn^{2+}]_{init}$ (μmol·L^{-1})	R_{SL} (g·L^{-1})	$[Na^+]$ (mol·L^{-1})	pH range	clay
B1	1.0			1.0	0.1	4.0−6.5	Kunipia-P
B2	1.1		110	1.0	0.1	4.0−6.5	Kunipia-P
B3	1.0	1.1		1.0	0.1	4.0−6.5	Kunipia-P
B4	1.1	9.8		1.0	0.1	4.0−6.5	Kunipia-P
B5	10.2			10.0	0.3	6.5−7.8	Kunipia-F
B6	10.2	7		10.0	0.3	6.5−7.8	Kunipia-F

(considered 2% of the values). Uncertainties on R_{SL} were neglected.

3.4. Overview of Adsorption/Desorption Experiments. Four types of experiments were set up to identify and quantify the effects of competition processes on Pb^{2+} and Co^{2+} adsorption on montmorillonite. All preparations and experiments were conducted at air atmosphere and at room temperature.

In a first set of experiments (Table 1), time-dependent adsorption/desorption experiments were conducted in which successive additions of Pb^{2+}, Mg^{2+}, and Zn^{2+} made it possible to quantitatively assess possible competition effects. These experiments were carried out in glass reactors containing a clay material dispersed in water at buffered pH (6.9 ± 0.1) and ionic strength (0.3 mol·L^{-1} NaCl) and with a solid concentration (R_{SL}) of ∼10 g·L^{-1}. 1 mmol·L^{-1} MOPS buffer was used in pH adjustment, and pH values were monitored during the experiments. The high ionic strength and the chosen pH value ensured that the contribution of cation exchange to the overall Pb^{2+} adsorption extent was negligible, and that observed concentration changes were related only to adsorption mechanisms taking place at edge surfaces. Total Pb^{2+} concentration was 10 μmol·L^{-1}. The chosen Pb^{2+} concentration to clay mass ratio (1 mmol·kg^{-1}) ensured also that investigated conditions corresponded to the reactivity of high affinity sites on edge surfaces.[30,41] The order of Pb^{2+} and Mg^{2+} additions in the clay dispersion was varied (Pb^{2+} before Mg^{2+} or Mg^{2+} before Pb^{2+}) in order to check the presence or absence of hysteretic effects on adsorption/competition processes. A pre-equilibration period before each additions enabled the systems to reach steady-state (1 week for Pb^{2+} adsorption and 3 days for Co^{2+} adsorption). This was also verified with sample aliquots taken before the competitor was added and with concentration measurement after ∼7 and ∼20 more days of interactions. The experiment conducted with Pb^{2+} addition before Mg^{2+} addition was duplicated, albeit with slightly different values of pH, total Pb^{2+} concentration, and added Mg^{2+} concentration, to check the reproducibility of the results (experiments K1a and K1b in Table 1). A second set of experiments was carried out with the same procedure as the first set but using Co^{2+} instead of Pb^{2+} (Table 1). Zn^{2+} was added in experiments K2 and K4 at step 3 in order to quantify competition between Pb^{2+} or Co^{2+} and Zn^{2+} with Mg^{2+} being already added to the systems.

A third set of experiments consisted in Pb^{2+} batch adsorption tests in the presence (experiments B3, B4, and B6) or absence (experiments B1 and B5) of added Mg^{2+} and in the presence (experiment B2) or absence (experiments B1 and B6) of added Zn^{2+}, as a function of pH from 6.5 to 8, and in the presence of a NaCl electrolyte with concentrations ranging from 0.1 to 0.3 mol·L^{-1}, solid concentrations ranging from 1 to 10 g·L^{-1}, and total Pb^{2+} concentrations ranging from 1 to 10 μmol·L^{-1} (Table 2).

At last, a fourth set of experiments was conducted in order to see the effect of Mg concentration onto Pb adsorption. It included Pb^{2+} adsorption/desorption tests as a function of Mg^{2+} concentration at buffered pH 7, and constant 0.3 mol·L^{-1} NaCl electrolyte background, with a solid concentration of 10 g·L^{-1} and an initial Pb^{2+} concentration of 10 μmol·L^{-1}.

3.5. Experimental Details on Adsorption−Desorption Experiments. *3.5.1. Time-Dependent Adsorption−Competition−Desorption Experiments.* 1 mmol·L^{-1} MOPS concentration was used to buffer pH, which was also monitored during the experiments. Clay dispersions were equilibrated for 1 week at the targeted pH in the presence of 0.3 mol·L^{-1} NaCl or 0.3 mol·L^{-1} NaCl + 10 mmol·L^{-1} $MgCl_2$, with continuous mixing using a magnetic stirrer. Then, sufficient amounts of a 1 mmol·L^{-1} Pb^{2+} stock solution was added into the reactors to reach the targeted total Pb^{2+} concentration. After 1 week of interaction, an adequate amount of 1 mol·L^{-1} Mg^{2+} stock solution or 12 mmol·L^{-1} Zn^{2+} stock solution was added into the reactor. Pb^{2+} desorption was monitored for two more days. A similar procedure was conducted to investigate Co^{2+} adsorption and desorption upon competition with Mg^{2+} and Zn^{2+}. Additions of solutions into the dispersions in the intermediate stages resulted in small dilutions that were taken into consideration in total initial concentration calculations.

Thermo Scientific Nalgene Oak Ridge high-speed polypropylene centrifuge tubes, 15 mL Falcon polypropylene centrifuge tubes, and glass reactors were acid treated (HNO_3) and washed three times with ultrapure water before usage. Acid-washed Falcon tubes were used for metal concentration measurements and water washed Falcon tubes were used for other measurements. After addition of Zn^{2+}, Mg^{2+}, Co^{2+}, or Pb^{2+}, sampling started after about 10 min of mixing. Before addition of Mg^{2+} or Zn^{2+}, one more sample was taken from the reactor, and it was kept until the end of the experiment in order to compare the adsorption/desorption rates with and without addition of Mg^{2+} or Zn^{2+}. At each sampling time, a 20 mL aliquot was taken out from the reactor and was centrifuged at 3000 g (Jouan CR3i centrifuge) in High-Speed Polypropylene centrifuge tubes, for 5 or 20 min depending on the clay sample and type of background electrolyte. Then, the supernatant was filtered by using a polypropylene syringe filter with 0.1 μm PTFE membranes (Merck, Omnipore). For Co^{2+}, Zn^{2+}, Pb^{2+}, and Mg^{2+} concentrations measurements, 5 mL of filtered solution was put into acid-washed Falcon tubes and 20 μmol·L^{-1} of HNO_3 (65%) was added into these tubes. The remaining filtered solution was put into water-washed Falcon tubes for other measurements.

3.5.2. Pb^{2+} Adsorption Tests as a Function of Mg^{2+} Concentration. Clay material was dispersed in a solution with 0.3 mol·L^{-1} NaCl background electrolyte and at R_{SL} of 10 g·L^{-1}. The pH value was adjusted to 7 by using 0.1 mol·L^{-1} HCl or mol·L^{-1} NaOH stock solutions in the presence of 1 mmol·L^{-1} MOPS buffer. After 1 week of equilibration, two sets

https://doi.org/10.1021/acsearthspacechem.1c00323
ACS Earth Space Chem. 2022, 6, 144−159

of nine samples were prepared from this clay suspension, and an adequate amount of 0.5 mol·L^{-1} $MgCl_2$ stock solution was added into each tube. The total concentration of Mg^{2+} in each set ranged between 0 and 7 mmol·L^{-1}. After 4 days of interaction (on horizontal shaker), the first set of the samples were centrifuged and filtered with the procedure mentioned before, and a sufficient amount of 1 mmol·L^{-1} Pb stock solution was added into the second set of samples to satisfy a 10 μmol·L^{-1} total Pb^{2+} concentration in each tube. These samples were agitated for 4 days more, and the supernatant was separated by centrifugation and filtration.

3.5.3. Batch Adsorption Tests. Clay stock dispersions with solid concentration (R_{SL}) of 2 g·L^{-1} were prepared in a 0.1 mol·L^{-1} NaCl solution. Thermo Scientific Nalgene Oak Ridge high-speed polypropylene centrifuge tubes were acid treated (HNO_3) and washed three times with ultrapure water before use. Then, to prepare 20 mL of adsorption sample 10 mL of the clay stock dispersion was mixed with 8 mL of the 0.1 mol·L^{-1} NaCl solution, and the pH was equilibrated from 4 to 6.5 by adding a 0.01 mol·L^{-1} or 0.1 mol·L^{-1} HCl solution, or of a 0.01 mol·L^{-1} or 0.1 mol·L^{-1} NaOH solution. Both HCl and NaOH solutions were prepared in a 0.1 mol·L^{-1} NaCl electrolyte background. Depending on the experiment, 0.2 mL of a 11 mmol·L^{-1} $ZnCl_2$ solution, or 0.2 or 0.02 mL of a 1.1 mol·L^{-1} $MgCl_2$ solution were added into the dispersion tubes. Then, 2 mL of acidified $PbCl_2$ stock solution (10 μmol·L^{-1}) was added to reach a final 1 μmol·L^{-1} total Pb^{2+} concentration. The tubes were closed hermetically and put onto a horizontal shaker (Heidolph Rotamax 120) for 4 days. Additionally, control samples were prepared for each of the experiment conditions. They were prepared with the same procedure except that the clay stock dispersion was replaced by NaCl stock solutions. The initial Pb^{2+} concentration ($[Pb^{2+}]_{init}$) was determined from the measured average Pb^{2+} concentrations in these control experiments at pH values below 6.5. After equilibration, samples were centrifuged at ∼12 700 g for 15 min (Sigma 6 K 10 Bioblock Scientific centrifuge). Then, a 5 mL aliquot of supernatant was acidified with ∼20 μL of 65% mol·L^{-1} HNO_3 in polystyrene tubes for Pb^{2+} measurements. Another 5 mL aliquot was preserved without acidification for other measurements. The volume of added HNO_3 solution was taken into account to correct the measurement of final Pb^{2+} concentration.

In a separated set of batch experiments, clay minerals were dispersed at 0.3 mol·L^{-1} NaCl background electrolyte concentration and at R_{SL} of 10 g·L^{-1}. The pH value was adjusted within the range of 6.5−8 by using 0.1 mol·L^{-1} HCl or 0.1 mol·L^{-1} NaOH stock solutions, in the presence of 1 mmol·L^{-1} MOPS buffer. After 1 week of equilibration, $PbCl_2$ and $MgCl_2$ were added to reach a total Pb^{2+} concentration of 10 μmol·L^{-1}, and a total Mg^{2+} concentration of 0 or ∼7 mmol·L^{-1}. Samples were shaken on the horizontal shaker for 4 days, then they were centrifuged and filtered with the procedure mentioned in the previous paragraph.

3.6. Scanning Transmission Electron Microscopy Imaging and Data Simulation. Structural characterization was performed using a Nion Ultra-STEM 200 operated at 100 kV in scanning transmission electron microscopy (STEM) mode. Data were collected both in bright-field, in medium-angle annular dark-field (MAADF), and high-angle annular dark-field (HAADF) conditions. The image quality was constrained by the beam-induced damage (typical total electron doses below 10^6 electrons·nm^{-2} are used to maintain the crystallinity) and the weak contrast associated with single-layered materials.

To determine the cis-vacant or trans-vacant nature of the clay, data were compared to images that were calculated using the QSTEM software[63] and structure models from Tsipursky and Drits.[48] In all samples, **a** and **b** were respectively 5.18 and 8.98 Å. α and γ were both equal to 90°. β was 99.11° for the cis-vacant structure and 101.27° for the trans-vacant one. As modeling the data acquired in this study required the calculation of the STEM images of an isolated layer, a "supercell" approach was used in which a single layer was extracted along *c*.

In the following, only calculations corresponding to the trans-vacant and one cis-vacant structure are shown, because calculations carried out for the second possible cis-vacant structure were not significantly different from those of the other cis-vacant structure.

Samples were prepared according to a method modified after Nadeau (1985).[64] Sample aliquots from a Pb^{2+} batch adsorption test were redispersed in an aqueous solution to satisfy a 0.05 g·L^{-1} solid concentration. The dispersion was sonicated for 15 min (ultrasonic bath Elmasonic P) to promote delamination of clay mineral layers. Twenty microliters of the dispersion were put onto a mica disc (Highest grade V1, 20 mm, TED Pella, INC) and dried one night under room conditions to obtain oriented clay particles. Then, the sample was put into an oven at 50 °C for one night and placed in a desiccator for cooling and then prevacuumed for 20 min by vacuum pump (Vacuubrand GMBH CO kg). The sample was coated with carbon at 5 nm thickness (Cressington 328UHR Carbon Coater). Carbon-coated mica samples were put into milli-Q water having a pH of 6.5 in order to separate carbon-coated clay particles from the mica disc. Carbon-coated clay particles were taken from the surface of the water and placed onto lacey carbon copper grid (LC200-CU).

3.7. Surface Complexation Modeling. *3.7.1. Geochemical Code and Thermodynamic Database.* An in-house version of PHREEQC code,[45,46,65] which had been modified to handle eq 1, was used to carry out the calculations with the thermodynamic database ThermoChimie_PHREEQC_eDH_v9b0.dat for aqueous species speciation.[66]

3.7.2. Modeling Strategy. Modeling of Pb^{2+} adsorption mechanisms was carried out in three stages: (1) Pb^{2+}, Mg^{2+} and Zn^{2+} specific adsorption model parameters were fitted using the data from the pH dependent competition experiments; (2) these parameters were used to predict the equilibrium data obtained in the competition kinetic experiments; (3) the robustness of the model was tested using literature data. A large set of possible surface complexation reactions (surface type, site type, reaction stoichiometry, and binding constants) were tested for Pb^{2+}, Zn^{2+}, and Mg^{2+} until a satisfactory agreement with the data was found. We observed that the simplest modeling assumption, which was adsorption of all different types of cations onto a single site, for which they competed, did not allow for a satisfactory fit of the data, that is, whatever was considered reaction stoichiometry. The most parsimonious model that we found required that Pb^{2+}, Zn^{2+}, and Mg^{2+} surface complexation took place on two types of edge functional groups: the $SaOH_3$ edge sites, which are the nonsubstituted sites (that is, the most abundant), and the $SeOH_3$ edge sites in which Al in the octahedral sheet are substituted with Fe(III). Stages (1) and (2) were iterated until a satisfactory agreement was reached for all conditions.

https://doi.org/10.1021/acsearthspacechem.1c00323
ACS Earth Space Chem. 2022, 6, 144−159

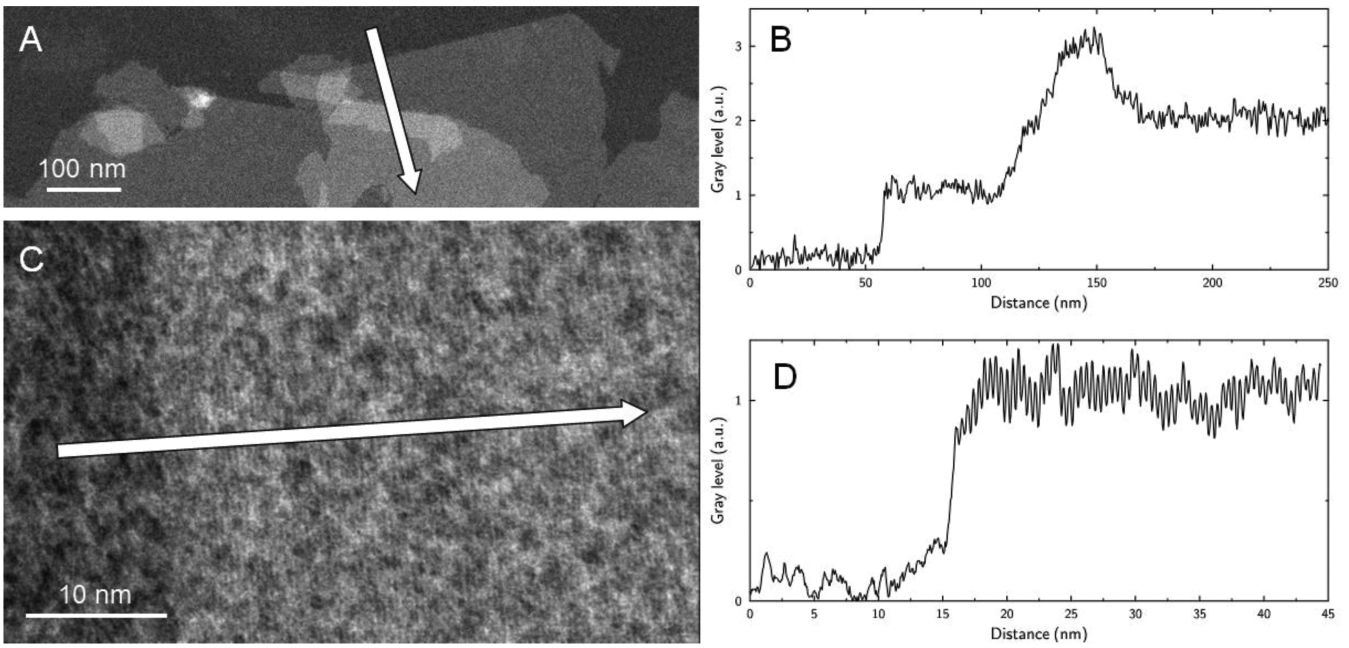

Figure 2. STEM imaging of clay particles. (A) STEM-HAADF image at low magnification showing the layers, seen perpendicular to the layer plane. (B) STEM-HAADF profile along the direction indicated by the arrow in panel A. The intensity offset have been roughly set to zero for the carbon film and the profile shows steps as a function of the numbers of layers. (C) STEM-HAADF image at the edge of a layer, seen perpendicular to the layer plane. (D) STEM-HAADF profile along the direction indicated by the arrow in panel C. The ∼0.45 nm periodicity is visible up to the surface plane. The small intensity decay at the last layers is due to the edge roughness and the integration width. The integration width for both profiles is 40 nm.

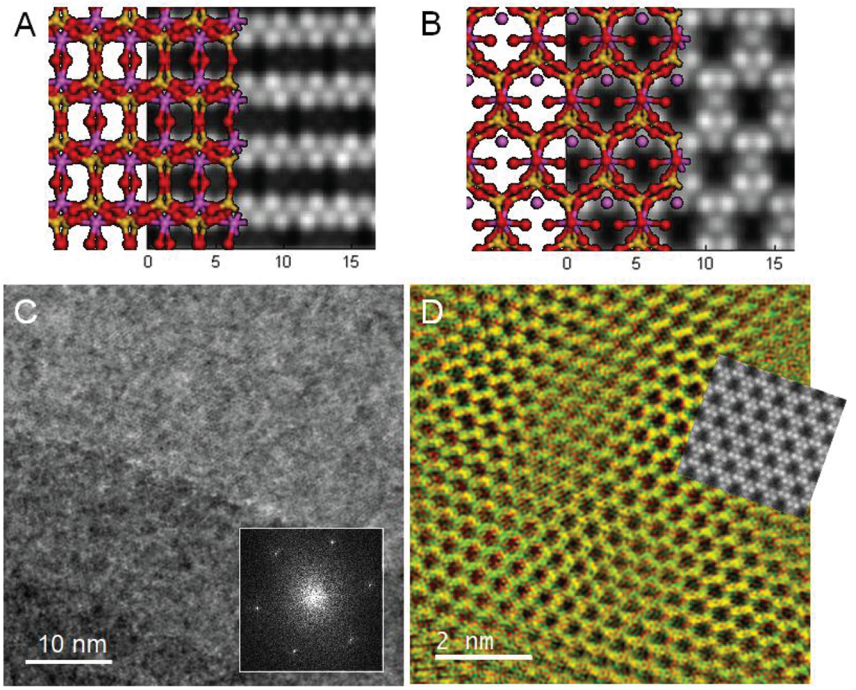

Figure 3. Top: atomic model and corresponding STEM-HAADF calculated images for trans-vacant (A) and cis-vacant (B) layer structures. Yellow, purple, and red balls are for, respectively, silicon, aluminum, and oxygen. The images are about 1.5 × 1.5 nm. Crystallographic planes are indicated on the cis-vacant structure. Bottom: (C) STEM-HAADF image containing a clay layer (top, light gray) and the amorphous carbon from the sample holder (bottom, dark gray). The fast Fourier transform of the clay is shown as an inset and is indexed for a [001] zone axis. Edge surface is of (110) type. (D) STEM-HAADF image of the clay shown in panel C after Fourier filtering. Calculated image for cis-vacant structure is overlapped.

3.7.3. Modeling Parameters. The presence of dissolved inorganic carbon (DIC) concentration of ∼0.25 mmol·L^{-1} and possible precipitation of hydrocerussite were considered in all samples, in agreement with our previous study on Pb^{2+} adsorption on montmorillonite.[67] For the competition experiments with Zn^{2+}, possible precipitation of hydrozincite ($Zn_5(OH)_6(CO3)_2$) was taken into consideration (its

https://doi.org/10.1021/acsearthspacechem.1c00323
ACS Earth Space Chem. 2022, 6, 144−159

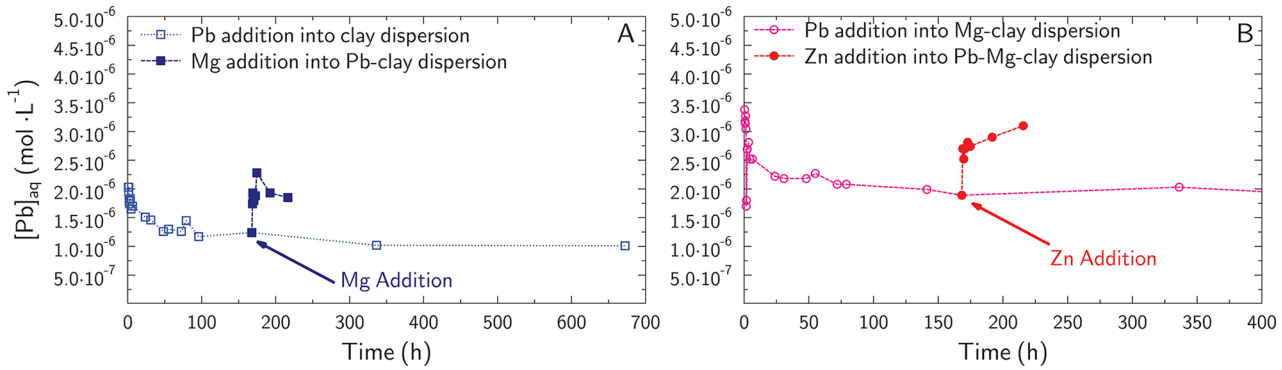

Figure 4. Time-dependent Pb^{2+} adsorption/desorption on/from Kunipia-F clay mineral surfaces at pH ∼6.9. The order of reagents additions is indicated in the inner caption. Experimental conditions are provided in Table 1 ((A) experiment K1a; (B) experiment K2). Closed symbols indicate that a competitor (Mg^{2+} and Zn^{2+} for panels A and B, respectively) was added at time ∼170 h. Note that Mg^{2+} was also added prior to Pb^{2+} for the experiment depicted in panel B.

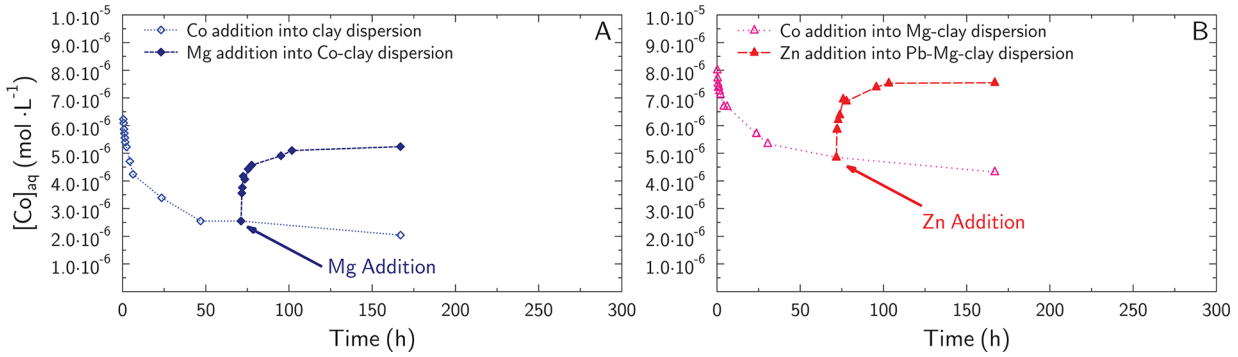

Figure 5. Time-dependent Co^{2+} adsorption/desorption on/from Kunipia-F clay mineral surfaces at pH ∼6.9. The order of reagents additions is indicated in the inner caption. Experimental conditions are provided in Table 1 ((A) experiment K3; (B) experiment K4). Closed symbols indicate that a competitor (Mg^{2+} and Zn^{2+} for panels A and B, respectively) was added at time ∼70 h. Note that Mg^{2+} was also added prior to Co^{2+} for the experiment depicted in panel B.

thermodynamic data was taken from the Thermoddem database at https://thermoddem.brgm.fr/).

Cation exchange capacity of Kunipia (P and F) was 1.15 $mol_c \cdot kg^{-1}$[68] and edge surface area was 5 $m^2 \cdot g^{-1}$.[60] After many model iterations, it was assumed on the basis of model fitting adequacy with the whole data set that surface complexation of the cations took place on two types of edge functional groups: the S_aOH_3 edge sites, which are the nonsubstituted sites (that is, the most abundant), and the S_eOH_3 edge sites in which Al in the octahedral sheet are substituted with Fe(III). A complete description of these sites is available in Tournassat et al.[45,46] and Zhang et al..[53]

4. RESULTS

4.1. STEM Observations. Precise description of edge surface sites is necessary to constrain our surface complexation model, which relies on the hypothesis of a crystalline nature of montmorillonite edges. STEM measurements made it possible to test this hypothesis and provided additional details on layer structure. At low magnification, clay layers had sizes in the layer plane (**ab** plane following the structure model from Tsipursky and Drits[48] roughly ranging between 10 and 1000 nm, Figure 2A). The presence of well-defined angles at the particle edges was often observed with the most often observed angle value being ∼120°, coherent with the expected layer symmetry,[48] assuming euhedral crystal. Under the microscope, a given layer had a given gray level, and when several layers were stacked, the gray level increased almost linearly with the number of layers (Figure 2A,B). This allowed selecting, for further structural investigations, regions if interest in which one single layer was present.

When observed along the [001] zone axis, a ∼0.45 nm periodicity, corresponding to either (020) or (110) planes with respectively 0.449 and 0.444 nm inter-reticular distances, was often observed in the clay layer (Figure 2C). This periodicity extended over the whole crystal, including at the layer edge (Figure 2D). This is interpreted as the clay layer edge having crystalline structure.

Finally, STEM observations were conducted at even higher magnification to determine if the clay sample had cis-vacant or trans-vacant layer structure. This, however, required first determining if this method could unambiguously identify them. For this purpose, images were calculated using the structure models from Tsipursky and Drits.[48] Whereas in HAADF imaging, the trans-vacant structure led to regular alternation of bright and dark lines (Figure 3A), because Si and Al atoms are segregated in "rows" when the structure is seen perpendicular to the layer plane, the calculated image from the cis-vacant structure was characterized by the presence of hexagonal shapes (Figure 3B). Because of the nearly hexagonal structure of the cis-vacant structure as observed along the [001] axis, (110), and (020) edges planes with zigzag structure and (100) and (130) edge planes with armchair structure can be defined (Figure 3B).

https://doi.org/10.1021/acsearthspacechem.1c00323
ACS Earth Space Chem. 2022, 6, 144−159

High-magnification images were then collected on clay layers with the observation vector being perpendicular to the layer plane. It was checked that the crystals on which data were collected were single layers by quantifying the gray level of the region of interest (as discussed above) but also by performing a fast Fourier transform analysis of the observation area (Figure 3C). The presence of hexagonal structures could be observed and matched the image calculated for the cis-vacant structure (Figure 3D). As observed for most of the flakes, the edge surface is of zigzag type with a crystallinity maintained up to the last plane.

To summarize, STEM observations allowed determining that the clay sample has a cis-vacant structure, with the crystals having well-defined angles at their edges and with these edges being crystallized, that is, having a structure resembling the ideal corresponding crystallographic planes. Collectively, all these observations support the idea that a surface complexation model based on crystallographic considerations can be safely applied to the present clay sample.

4.2. Competitive Adsorption/Desorption Experiments. Competitive adsorption/desorption kinetic experiments exhibited similar observation patterns for Pb^{2+} or Co^{2+} competitive adsorption with Mg^{2+} (Figure 4 and Figure 5; note that the *y*-axes have different scales on these two figures). In the absence of Mg^{2+} addition (Figure 4A and Figure 5A), Pb^{2+} and Co^{2+} aqueous concentrations decreased in solution down to 1 $\mu mol \cdot L^{-1}$ and 2 $\mu mol \cdot L^{-1}$ from 11.4 $\mu mol \cdot L^{-1}$ and 12 $\mu mol \cdot L^{-1}$ respectively, thus evidencing a higher adsorption for Pb^{2+} than for Co^{2+}. The stabilization of Pb^{2+} and Co^{2+} aqueous concentrations took approximately 4 days. Following Mg^{2+} addition, Pb^{2+} and Co^{2+} aqueous concentrations increased by a factor of two (Figure 4A and Figure 5A), thus evidencing their desorption from the clay and hence a competitive effect of Mg^{2+} on both Pb^{2+} and Co^{2+} adsorption. The same observations were made in experiment K1b (Supporting Information, Figure S1). Interestingly, in experiments carried out with Mg^{2+} added prior to Pb^{2+} (Figure 4B), Pb^{2+} aqueous concentration reached a steady-state value comparable to that measured after Mg^{2+} addition in the previous experiment (compare concentration levels on left and right figure). The same observation was made with Co^{2+} (Figure 5B). Consequently, the competitive effect of Mg^{2+} on Pb^{2+} or Co^{2+} adsorption was not dependent on the reagent addition order (for example, Pb^{2+}/Co^{2+} then Mg^{2+} vs Mg^{2+} then Pb^{2+}/Co^{2+}). At last, Zn^{2+} addition led to Pb^{2+} and Co^{2+} desorption similar to or greater than that observed with Mg^{2+} addition, although Zn^{2+} added concentration was 100 times smaller than Mg^{2+} addition (Figure 4B and Figure 5B), pointing out the lesser efficiency of Mg^{2+} compared to Zn^{2+} to displace Pb^{2+} and Co^{2+} from the surface.

In batch experiments at fixed pH, increased Mg^{2+} aqueous concentrations led to increased Pb^{2+} aqueous concentrations, thus evidencing, again, a competitive effect of Mg^{2+} on Pb^{2+} adsorption (Figure 6).

In batch adsorption experiments conducted as a function of pH, the addition of Mg^{2+} (and Zn^{2+}) competitors led to a decrease of Pb^{2+} adsorption, which was more pronounced for experiments conducted with a total Pb^{2+} concentration of 1 $\mu mol \cdot L^{-1}$ than with a total Pb^{2+} concentration of 10 $\mu mol \cdot L^{-1}$ (Figure 7). The corresponding R_D decrease was significant at pH values above ~5−5.5 only, at which surface complexation mechanisms were responsible for the observed retention. The maximum magnitude of R_D decrease amounted to a factor 4,

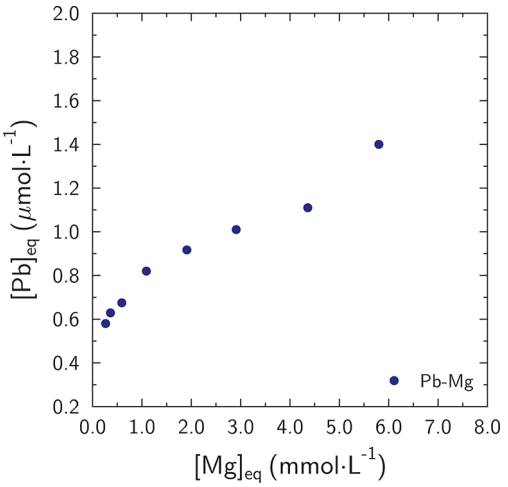

Figure 6. The influence of Mg^{2+} concentration on Pb^{2+} equilibrium concentration in batch adsorption experiments at pH 7 with 10 $g \cdot L^{-1}$ Kunipia-F and an initial Pb^{2+} concentration of 10 $\mu mol \cdot L^{-1}$ in the presence of 0.3 $mol \cdot L^{-1}$ NaCl.

which was beyond the errors bands associated to the adsorption data.

5. MODELING AND DISCUSSION

5.1. Cation Exchange on Planar Surfaces versus Surface Complexation on Edge Surfaces. Experimental data showed unambiguously the competition of Mg^{2+} with Pb^{2+} and Co^{2+} for adsorption sites. Mg^{2+} competition was also less efficient than Zn^{2+} competition for Pb^{2+} and Co^{2+} displacement from the surface. Batch adsorption/desorption experiments give no information about the type of adsorption site impacted by this competition process, and two categories of sites can be hypothesized: cation exchange sites on the planar surfaces of montmorillonite layers and surface complexation sites on the edge surfaces.[30] On the basis of known selectivity coefficients of Pb^{2+}, Mg^{2+}, and Zn^{2+} for cation exchange (Table 3), it can be calculated that Pb^{2+} and Co^{2+} in cation exchange position amounted for less than 3×10^{-6} $mol \cdot kg_{clay}^{-1}$, *i.e.* less than 3×10^{-8} $mol \cdot L^{-1}$ in our experimental conditions with 0.3 $mol \cdot L^{-1}$ NaCl electrolyte. Pb^{2+} and Co^{2+} concentration increases following Mg^{2+} addition (Figure 4 and Figure 5) amounted for 0.5×10^{-6} to 2×10^{-6} $mol \cdot L^{-1}$. Consequently, competition for cation exchange sites cannot be responsible for our experimental observations, leaving surface complexation sites as the preferred location for the competition processes evidenced in our experiments. The competition was also greater in the system $Mg^{2+}-Co^{2+}$ than in the system $Mg^{2+}-Pb^{2+}$. Pb^{2+} and Co^{2+} selectivity coefficients for exchange sites are similar, but Co^{2+} has a significantly weaker affinity compared to Pb^{2+} for clay mineral edge sites.[24,41] Differences in $Mg^{2+}-Co^{2+}$ and $Mg^{2+}-Pb^{2+}$ competition experiments are thus also in agreement with an effective competition of Mg^{2+} for adsorption on montmorillonite edge surface sites.

5.2. Competition Mechanism(s). Competition for adsorption on the same edge surface sites has already been put forward in previous studies to explain the selective competition processes between cations such as Ni^{2+}, Co^{2+}, Pb^{2+}, and Zn^{2+}, which undergo very selective and pH-dependent adsorption behaviors on montmorillonite edge surfaces.[22,24,39,41] For example, Marques Fernandes and

https://doi.org/10.1021/acsearthspacechem.1c00323
ACS Earth Space Chem. 2022, 6, 144−159

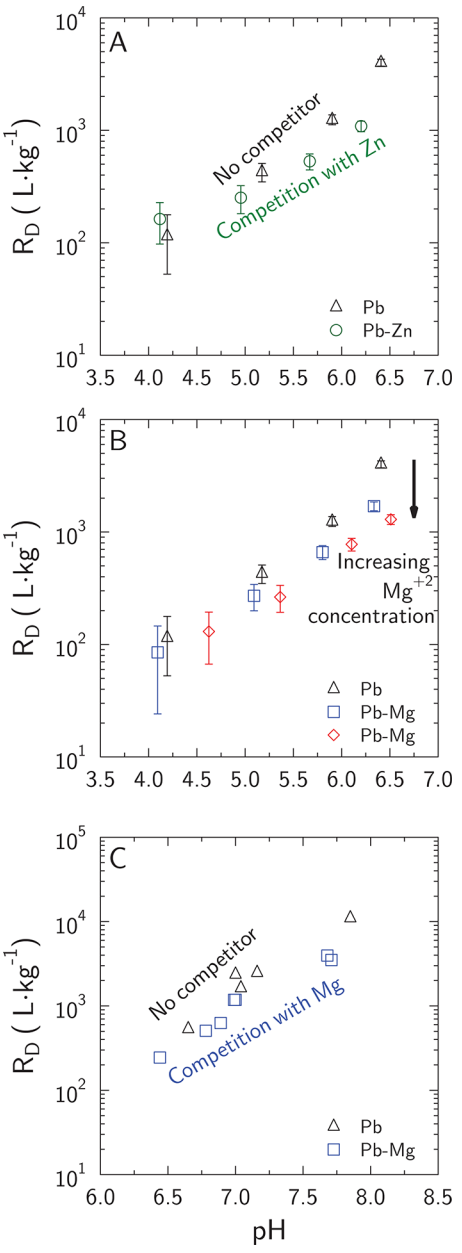

Figure 7. Mg^{2+} and Zn^{2+} competition with Pb^{2+} for adsorption on Kunipia-F in the presence of 0.1 mol·L^{-1} NaCl as a function of pH. Experimental conditions are provided in Table 2. (A) Black triangles = experiment B1; green circles = experiment B2. (B) Black triangles = experiment B1; blue squares = experiment B3; red diamonds = experiment B4. (C) Black triangles = experiment B5; blue squares = experiment B6.

Baeyens[24] modeled their Pb^{2+} adsorption data, including competition with Ni^{2+}, Co^{2+}, Zn^{2+}, and Eu^{3+}, with a multisite model in which only a fraction of surface sites was prone to competition effects. While spectrometric data such as polarized extended X-ray absorption fine structure (EXAFS) data coupled to ab initio molecular dynamics enabled one to confirm the location of, for example, Zn^{2+} adsorption on clay mineral edges[23,72] the exact nature of the competition mechanisms has not been evidenced with direct spectrometric measurements yet. In our study, because Mg^{2+} is a major component in montmorillonite layer structure, Mg^{2+} adsorption on clay edge surfaces is expected to result in very weak

Table 3. Cation Exchange Selectivity Coefficients on Montmorillonite Surfaces, Given in Gaines and Thomas[69] Thermodynamic Convention[a]

exchange reaction	log K
2 XNa + Mg^{2+} = X_2Mg + 2 Na^+	0.50[b]
2 XNa + Pb^{2+} = X_2Pb + 2 Na^+	0.60[c]
2 XNa + Zn^{2+} = X_2Zn + 2 Na^+	0.45[d]
2 XNa + Co^{2+} = X_2Co + 2 Na^+	0.57[e]

[a]X^- represents a cation exchange site. [b]Selectivity coefficient values are from Tournasat et al.[70] [c]Selectivity coefficient values are from Orucoglu et al.[67] [d]Selectivity coefficient values are from this study. [e]Selectivity coefficient values are from Bradbury and Baeyens.[71]

Table 4. Surface Complexation Modeling Parameters Used for Competitive Pb^{2+} Sorption Montmorillonite[a]

protonation/deprotonation reactions[b]	log K				
	S_a				S_e
	[010]	[110]			[010]
$>SOH_4^+$ = $>SOH_3$ + H^+	−3.1	−1.7			−1.2
$>SOH_3$ = $>SOH_2^-$ + H^+	−7	−5.5			−5.1
$>SOH_2^-$ = $>SOH^{-2}$ + H^+	−7	−8.3			−8.6
$>SOH^{-2}$ = $>SO^{-3}$ + H^+	−8.3	−8.3			−8.6
	S_b		S_c	S_d	
	[010]	[110]	[010]	[010]	[110]
$>SOH_4$ = $>SOH_3^-$ + H^+	−10.8	−4.2	−6.6	−4.9	2.4
$>SOH_3^-$ = $>SOH_2^{-2}$ + H^+	−10.8	−11	−10.2	−7	−10.2
$>SOH_2^{-2}$ = $>SOH^{-3}$ + H^+	−13.2	−11	−10.2	−8.5	−12.7
$>SOH^{-3}$ = $>SO^{-4}$ + H^+	N.A.	N.A.	−11.2	−15.1	−17.5
Pb^{2+}, Mg^{2+}, and Zn^{2+} adsorption reactions on S_a and S_e					
	S_a				.
	[010]	[110]			[010]
$>SOH_3$ + Pb^{2+} = $>SOH_2Pb^+$ + H^+	−2	−1.7			0.6
$>SOH_2Pb^+$ + H_2O = $>SOH_2PbOH$ + 2 H^+	−6.7				
$>SOH_3$ + Mg^{2+} = $>SOH_2Mg^+$ + H+	−6.5	−5.2			
$>SOH_3$ + Zn^{2+} = $>SOH_2Zn^+$ + H^+					−1.5

[a]Protonation and deprotonation of the functional groups for two different orientation were taken from the generic surface complexation model developed by Tournassat et al.[45] Pb^{2+}, Mg^{2+}, and Zn^{2+} surface complexation reaction constants were obtained by fitting of the experimental data. [010] and [110] indicate the crystallographic direction perpendicular to the edge surface. [b]From ref 45; N.A.: Not applicable

and thus barely detectable, changes in the average Mg^{2+} structural environment that could be probed with spectrometric or diffractometric techniques. Consequently, our current understanding of adsorption competition mechanisms on clay edge surfaces relies mostly on indirect information obtained from surface complexation modeling of adsorption data.

While direct competition of two species for adsorption on the same adsorption site is a straightforward explanation for the observed adsorption/desorption data, adsorption onto different but neighboring sites can also be responsible for the overall adsorption competition at the surface. The latest mechanism can alter the local edge structure, and/or the local electrostatic field, thus partly inhibiting adsorption of a species

https://doi.org/10.1021/acsearthspacechem.1c00323
ACS Earth Space Chem. 2022, 6, 144−159

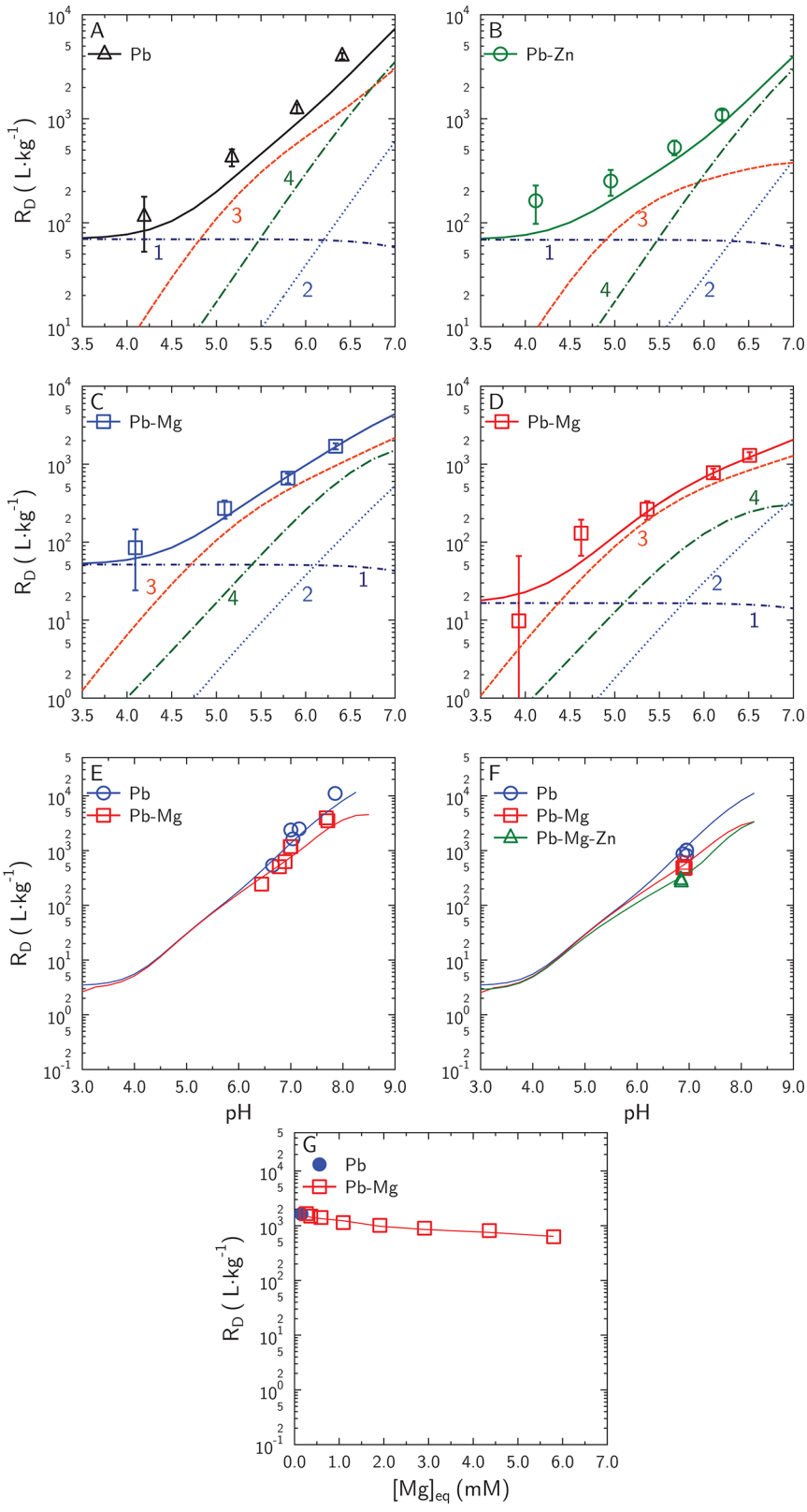

Figure 8. Surface complexation modeling of pH-dependent adsorption of Pb^{2+} in the presence or absence of added Mg^{2+} and Zn^{2+}. Experimental conditions are provided in Table 1 and Table 2. Panel A: experiment B1. Panel B: experiment B2. Panel C: experiment B3. Panel D: experiment B4. Panel E: experiment. B5, blue circle and experiment B6, red-square. Panel F: experiment K1a step 2, blue circle and experiment K1a step 3, red square, and experiment K2 green triangle in Table 1. Panel G: Pb^{2+} adsorption onto Kunipia-F under the influence of Mg^{2+} concentration in the presence of 0.3 mol·L^{-1} NaCl at pH 7. Symbols: experimental data. Full lines: model prediction. Dashed lines: modeled site contributions to overall adsorption (1, cation exchange; 2, $[010]SO_aH_2Pb^+$; 3, $[010]SO_eH_2Pb^+$; 4, $[110]SO_aH_2Pb^+$).

https://doi.org/10.1021/acsearthspacechem.1c00323
ACS Earth Space Chem. 2022, 6, 144−159

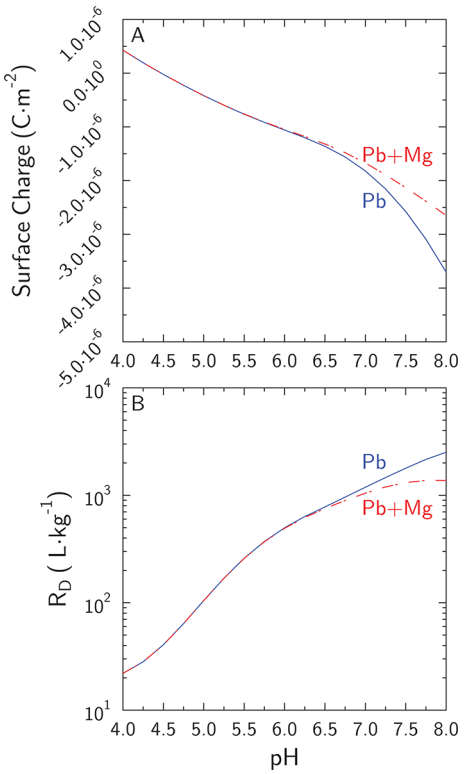

Figure 9. Influence of the addition of 10 mmol·L^{-1} Mg^{2+} on surface charge (A) and 1 μmol·L^{-1} Pb^{2+} adsorption (B) for the edge surface perpendicular to the [010] crystallographic direction.

upon adsorption of another species at a different site, as observed on iron oxides and kaolinite.[73−75] Nonelectrostatic models such as the 2SPNE SC/CE model[24] cannot be used to test the possibility of such a competition mechanism because of the absence of an electrostatic contribution to the species affinity for the surface. Consequently, we used an electrostatic model to test the latest competition mechanism.

5.3. Modeling of Competition Processes with a State-of-the Art Electrostatic Surface Complexation Model. Results obtained with model parameters from Table 3 and Table 4 confirmed that cation exchange sites did not account for a significant share in the competition processes at pH > 5 (Figure 8A−D). The best fit of the data was obtained with the hypothesis that Pb^{2+} was adsorbed predominantly onto the S_e substituted sites ($S_eOH_2Pb^+$ on the surface perpendicular to the [010] direction, (Figure 8A−D). The influence of Zn^{2+} competition was well described by a site occupancy effect (Figure 8B) with Pb^{2+} being adsorbed predominantly onto the available nonsubstituted S_a sites. In the presence of Mg^{2+}, the model also predicted a decrease of Pb^{2+} adsorption on the S_e substituted sites (Figure 8C,D) although Mg^{2+} was not allowed to adsorb on these sites (Table 4). Changes in Pb^{2+} adsorption were the results of changes in electrostatic properties of the surface upon Mg^{2+} adsorption at S_a sites (the surface became less negative), leading to a decrease of Pb^{2+} adsorption on neighboring S_e sites (Figure 9A,B). This mechanism made it also possible to model Pb^{2+} adsorption data as a function of Mg^{2+} concentration (Figure 8G). Additionally, data measured at steady state in the kinetic competition experiments were well predicted with this model (Figure 8E,F).

Our model contained seven adjusted log K parameters to reproduce the competitive adsorption of three aqueous species on the montmorillonite edge surfaces. All other parameters were obtained from direct measurements or independent models such as first principle molecular dynamics (FPMD).[45,46,53] In the proposed electrostatic model, an important assumption is the crystalline nature of clay edge surfaces for which a structure identical to the bulk layer structure was considered to calculate protonation−deprotonation reaction constant using FPMD techniques.[4,54−56,76] Our HR-STEM results provide a strong case of the adequacy of the crystallinity assumption. Besides, recent atomic force microscopy measurements enabled to quantify the preferential orientation of Kunipia montmorillonite edge surfaces,[60] and results were in good agreement with the average orientation considered in our model. While these findings support the adequacy of the proposed model, the number of possible site combinations for Pb^{2+}, Mg^{2+}, and Zn^{2+} adsorption makes it impossible to warrant unicity of the model parameters, and different combinations of adsorption and log K values may be as effective as the set of parameters fitted in this study. The reliability of the proposed model was thus blind-tested on

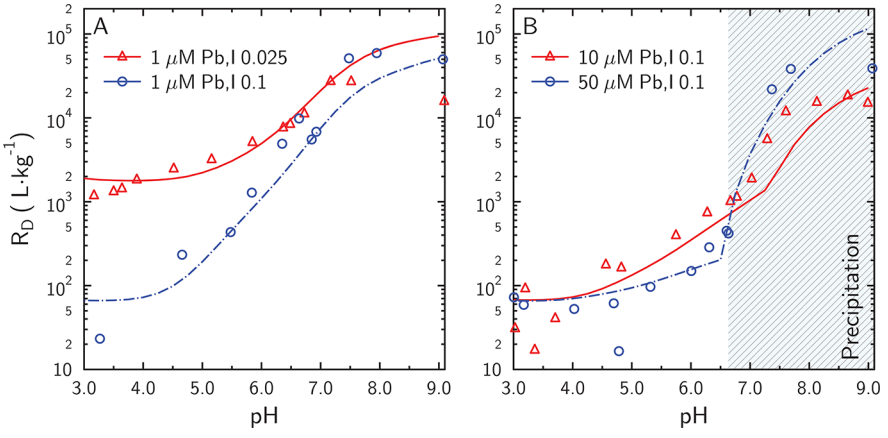

Figure 10. Model predictions (lines) of Pb^{2+} adsorption data (symbols) on Kunipia-P from Orucoglu et al.[67] (A) Pb^{2+} (1 μmol·L^{-1}) in the presence of 0.025 mol·L^{-1} NaCl (red triangles and red full line) and 0.1 mol·L^{-1} NaCl (blue circles and blue dashed line). (B) Pb^{2+} (10 μmol·L^{-1} (red triangles and red full line) and 50 μmol·L^{-1} (blue circles and blue dashed line)) in the presence of 0.01 mol·L^{-1} NaCl. Dashed area (////) highlights the pH region in which hydrocerussite ($Pb_3(CO_3)_2(OH)_2$) precipitation was expected at 50 μM Pb^{2+} total concentration..

https://doi.org/10.1021/acsearthspacechem.1c00323
ACS Earth Space Chem. 2022, 6, 144−159

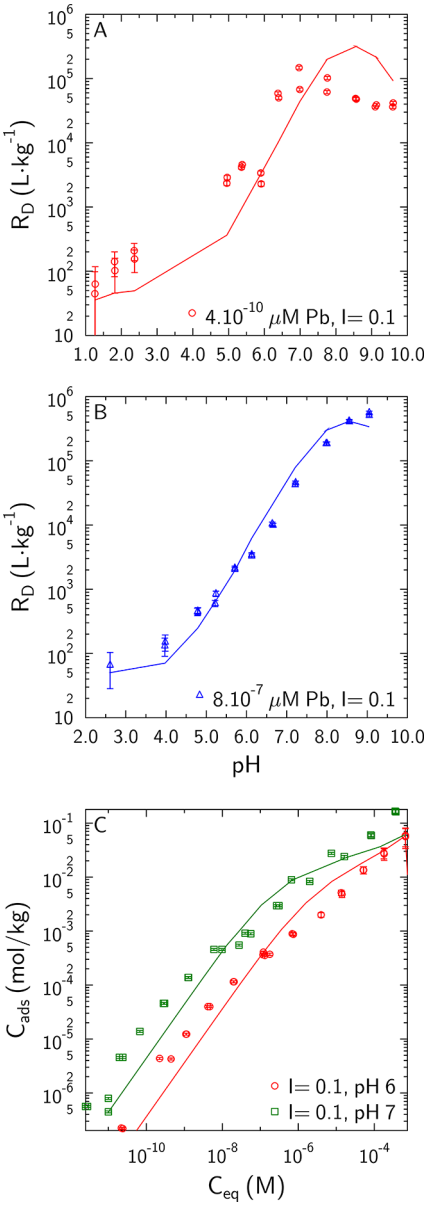

Figure 11. Model prediction (lines) of Pb^{2+} adsorption data (symbols) on SWy-2 montmorillonite from Marques Fernandes and Baeyens.[24] (A) Pb^{2+} (4×10^{-4} μmol·L^{-1}) in the presence of 0.1 mol·L^{-1} NaCl; (B) 0.8 μmol·L^{-1} Pb^{2+} in the presence of 0.1 mol·L^{-1} NaCl; (C) adsorption isotherm at pH 6 (red circles and red full line) and pH 7 (green squares and dashed lines) in the presence of 0.1 mol·L^{-1} NaCl.

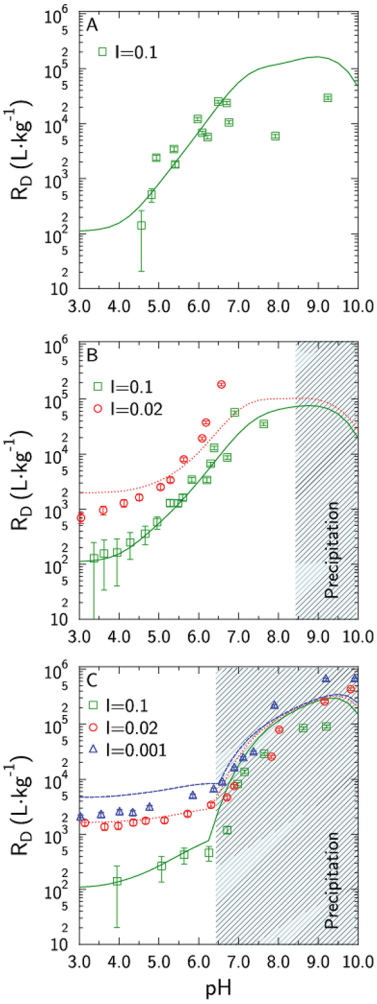

Figure 12. Model (lines) prediction of Pb^{2+} adsorption data (symbols) on SWy-2 montmorillonite from Akafia et al.[27] at three Pb^{2+} total concentrations (A) 0.5 μmol·L^{-1}, (B) 5 μmol·L^{-1}, and (C) 50 μmol·L^{-1}) and three ionic strength values (green squares and green full line, 0.1 mol·L^{-1} NaCl; red circles and red dotted line, 0.02 mol·L^{-1} NaCl; blue triangles and blue dashed line, 0.001 mol·L^{-1} NaCl).

additional Pb^{2+} adsorption data obtained from the literature to check its applicability in a wider range of conditions.

Our model successfully reproduced most of Pb^{2+} adsorption data from Orucoglu et al.[67] (Figure 10) for which Mg^{2+} aqueous concentrations were estimated as a function of pH on the basis of measurements made in the present study (Supporting Information, Figure S2 and data tables S1−S14). Adsorption at low ionic strength at pH value above 7 was overestimated though, because of an increased contribution of the surface potential term in the adsorption reaction at low ionic strength.[30] Actually, our iterative modeling tests showed that the consideration of Mg^{2+} adsorption onto edge surfaces improved significantly the prediction at low ionic strength compared to a model without Mg^{2+} adsorption. This reinforced our interpretation that Mg^{2+} adsorption had an indirect effect on Pb^{2+} adsorption, which was mediated by changes in the electrostatic field.

A blind prediction of the model was also carried out on Pb^{2+} adsorption data from Marques Fernandes and Baeyens,[24] which was obtained on an acid-washed homoionic sodium SWy-2 montmorillonite. Since the adsorption edge and isotherms at pH 6 and 7 were measured in a controlled N_2 atmosphere glovebox, dissolved inorganic carbon was considered negligible and hydrocerussite precipitation was not considered in the simulations. Mg^{2+} and Zn^{2+} concentrations at equilibrium were not reported in the reference study and it was assumed that SWy-2 clay had 5 mmol·kg^{-1} Mg^{2+} and 1 mmol·kg^{-1} Zn^{2+}, which could desorb from the surface, in agreement with previous investigations.[77] An edge specific surface area of 25 m^2·g^{-1} and a CEC of 0.87 mol$_c$·kg^{-1} were used, in agreement with the reported range of measured values for SWy-2.[45,78,79] Despite differences in the nature of the investigated clay mineral sample, our model was able to predict Pb^{2+} adsorption data adequately without the requirement to adjust any parameter proposed in Table 4 (Figure 11).

https://doi.org/10.1021/acsearthspacechem.1c00323
ACS Earth Space Chem. 2022, 6, 144−159

Finally, an additional blind prediction was carried out with the data from Akafia et al.,[27] obtained on a raw SWy-2 material. We considered Mg^{2+}, Zn^{2+} and DIC concentrations of 120 $mmol{\cdot}kg_{clay}^{-1}$, 1 $mmol{\cdot}kg_{clay}^{-1}$, and 0.25 $mmol{\cdot}L^{-1}$ respectively, together with the same specific edge surface area and CEC as those used to model the data of Marques Fernandes and Baeyens.[24] A high concentration of Mg^{2+} was used because Akafia et al.[27] used a raw SWy-2 material. The sources for this higher Mg^{2+} content could be clay exchangeable cations, dissolution of impurity minerals like dolomite and partial dissolution of clay minerals.[67] For example, Baeyens and Bradbury[77] measured a 10-fold higher Mg^{2+} concentration on a raw SWy-1 material compared to their purified material following an acid extraction procedure (110 $mmol{\cdot}kg^{-1}$ and 11 $mmol{\cdot}kg^{-1}$, respectively). Adsorption data were well predicted for a large range of Pb^{2+} concentrations especially in the presence of 0.1 $mol{\cdot}L^{-1}$ NaCl (Figure 12) but successful data reproduction required considering hydrocerussite precipitation at pH > 6.5 and for total Pb^{2+} concentration of 50 $\mu mol{\cdot}L^{-1}$, in agreement with findings of Orucoglu et al.[67]

Our electrostatic model is specific of the acid−base chemistry of montmorillonite in NaCl dominated electrolyte.[45] In order to apply the model to other types of electrolytes, dominated, for example, by Mg^{2+} or Ca^{2+}, it may be necessary to investigate further the effect of divalent cations on the charge and potential of montmorillonite edge surfaces.

6. CONCLUSION

Our experimental results showed unambiguously the influence of the Mg^{2+} concentration level on the specific adsorption of Pb^{2+} and Co^{2+} on clay mineral edge surfaces. In the clay adsorption literature, the possibility that major cations present in natural waters can influence specific surface complexation processes is generally not considered. The role of Mg^{2+} on overall metal or radionuclide adsorption is usually relegated to competition processes for cation exchange sites on basal surfaces only. Our experimental results could not be explained without a specific adsorption mechanism for Mg^{2+} on the clay mineral edge surfaces, and this hypothesis was supported by successful data modeling. This result is also in agreement with the facts that Mg^{2+} is a major component of the octahedral sheet of the montmorillonite layer and that adsorption processes on clay mineral edges may be described as a possible initiation of an epitaxial growth of clay mineral layers.[80] The maximum Mg^{2+} concentration value investigated in the present study (10 $mmol{\cdot}L^{-1}$) is commensurate with the range of concentration commonly observed in clay sedimentary rocks or in marine sediment pore waters.[81] One can thus anticipate that the Mg^{2+} competition effect observed in our experiment applies also in most of clayey natural environments. A direct consequence of this conclusion is that the adsorption data obtained on pure clay mineral phases, and the models that have been built using these data may overestimate the retention properties of these clay mineral phases when applied to natural environments.

From a methodological point of view, our results highlight the need to systematically quantify the full solution composition in order to build a comprehensive understanding of the processes at work adsorption experiments, if one wants to apply bottom-up approaches to model retention properties in natural systems. In the presence of high concentration of adsorbed element, our previous work already highlighted the need to measure dissolved organic carbon to help decipher true adsorption processes from (co)precipitation processes in metals retention data[67] or to build parsimonious models for the adsorption of element with a complex solution speciation such as uranium.[46] The need to collect data on competing trace elements was already put forward in a number of other studies.[24,41,82,83] In the present study, we extended this need to the measurement of minor or major elements such as Mg^{2+}.

On a modeling point of view, our study showed that adsorption competition processes are not necessarily due to simple competition for site occupancy, but they can also be triggered by changes in surface potential following adsorption on neighboring sites. This conclusion points out to the need of a comprehensive understanding of surface adsorption processes on clay mineral edges, taking into account the full complexity of the site's nature and distribution as well as of electrostatic interactions between them.

■ ASSOCIATED CONTENT

Supporting Information

The Supporting Information is available free of charge at https://pubs.acs.org/doi/10.1021/acsearthspacechem.1c00323.

> Time-dependent adsorption of 10 $\mu mol{\cdot}L^{-1}$ Pb^{2+} on Kunipia-F clay mineral surfaces (Figure 1), measured Mg^{2+} and Zn concentrations at equilibrium in a subset of pH-dependent Pb adsorption samples (Figure 2), measurements of time-dependent adsorption/desorption experiments (Tables 1−10), measurements of pH-dependent adsorption/desorption experiments (Table 11−14) (PDF)

■ AUTHOR INFORMATION

Corresponding Author

Esra Orucoglu − *Institut des Sciences de la Terre d'Orléans, UMR 7327 Université d'Orléans−CNRS/INSU−BRGM, 45071 Orléans, France; BRGM, 45060 Orléans, France;* orcid.org/0000-0002-8916-5463; Email: e.orucoglu@brgm.fr

Authors

Sylvain Grangeon − *BRGM, 45060 Orléans, France;* orcid.org/0000-0002-5018-3015

Alexandre Gloter − *Laboratoire de Physique des Solides, Université Paris-Saclay, 91405 Orsay, France;* orcid.org/0000-0002-4813-3799

Jean-Charles Robinet − *Andra, R&D Division, 92298 Châtenay-Malabry, France*

Benoît Madé − *Andra, R&D Division, 92298 Châtenay-Malabry, France*

Christophe Tournassat − *Institut des Sciences de la Terre d'Orléans, UMR 7327 Université d'Orléans−CNRS/INSU−BRGM, 45071 Orléans, France; BRGM, 45060 Orléans, France; Earth and Environmental Sciences Area, Lawrence Berkeley National Laboratory, Berkeley, California 94720, United States*

Complete contact information is available at: https://pubs.acs.org/10.1021/acsearthspacechem.1c00323

Notes

The authors declare no competing financial interest.

■ ACKNOWLEDGMENTS

This work was mainly supported by the French Radioactive Waste Management Agency (Andra) as part of the Andra-BRGM scientific partnership (CTEC project). Additional fundings from the EC Horizon 2020 project EURAD under Grant Agreement 847593 (WP FUTURE) and from a grant overseen by the French National Research Agency (ANR) as part of the "Investissements d'Avenir" Programme LabEx VOLTAIRE, 10-LABX-0100 are acknowledged. We gratefully acknowledge Prof. Tsutomu Sato from Hokkaido University for providing the Kunipia samples. The authors acknowledge support from the CNRS-CEA "METSA" French network (FR CNRS 3507) on the LPS plateform.

■ REFERENCES

(1) Bárcena, J. F.; Claramunt, I.; García-Alba, J.; Pérez, M. L.; García, A. A method to assess the evolution and recovery of heavy metal pollution in estuarine sediments: Past history, present situation and future perspectives. *Mar. Pollut. Bull.* **2017**, *124*, 421−434.

(2) Vareda, J. P.; Valente, A. J.M.; Duraes, L. Assessment of heavy metal pollution from anthropogenic activities and remediation strategies: A review. *J. Environ. Manage.* **2019**, *246*, 101−118.

(3) Xu, D.; Tan, X. L.; Chen, C. L.; Wang, X. K. Adsorption of Pb(II) from aqueous solution to MX-80 bentonite: Effect of pH, ionic strength, foreign ions and temperature. *Appl. Clay Sci.* **2008**, *41*, 37−46.

(4) Zhang, C.; et al. Surface complexation of heavy metal cations on clay edges: insights from first principles molecular dynamics simulation of Ni(II). *Geochim. Cosmochim. Acta* **2017**, *203*, 54−68.

(5) Zhu, J.; et al. Sorption of Cu, Pb and Cr on Na-montmorillonite: Competition and effect of major elements. *Chemosphere* **2011**, *84*, 484−489.

(6) Kul, A. R.; Koyuncu, H. Adsorption of Pb(II) ions from aqueous solution by native and activated bentonite: Kinetic, equilibrium and thermodynamic study. *J. Hazard. Mater.* **2010**, *179*, 332−339.

(7) Wang, S.; Dong, Y.; He, M.; Chen, L.; Yu, X. Characterization of GMZ bentonite and its application in the adsorption of Pb(II) from aqueous solutions. *Appl. Clay Sci.* **2009**, *43*, 164−171.

(8) Bradl, H. B. Adsorption of heavy metal ions on soils and soils constituents. *J. Colloid Interface Sci.* **2004**, *277*, 1−18.

(9) Nagajyoti, P. C.; Lee, K. D.; Sreekanth, T. V. M. Heavy metals, occurrence and toxicity for plants: a review. *Environ. Chem. Lett.* **2010**, *8*, 199−216.

(10) Wuana, R. A.; Okieimen, F. E. Heavy metals in contaminated soils: a review of sources,chemistry, risks and best available strategies for remediation. *ISRN Ecology* **2011**, *2011*, 1−20.

(11) Echeverria, J. C.; Morera, M. T.; Mazkiaran, C.; Garrido, J. J. Competitive sorption of heavy metal by soils. Isotherms and fractional factorial experiments. *Environ. Pollut.* **1998**, *101*, 275−284.

(12) Serrano, S.; O'Day, P. A.; Vlassopoulos, D.; García-González, M. T.; Garrido, F. A surface complexation and ion exchange model of Pb and Cd competitive sorption on natural soils. *Geochim. Cosmochim. Acta* **2009**, *73*, 543−558.

(13) Baeyens, B.; Bradbury, M. H. A mechanistic description of Ni and Zn sorption on Na-montmorillonite. Part I: Titration and sorption measurements. *J. Contam. Hydrol.* **1997**, *27*, 199−222.

(14) Covelo, E. F.; Vega, F. A.; Andrade, M. L. Competitive sorption and desorption of heavy metals by individual soil components. *J. Hazard. Mater.* **2007**, *140*, 308−315.

(15) Sipos, P.; Németh, T.; Kis, V. K.; Mohai, I. Sorption of copper, zinc and lead on soil mineral phases. *Chemosphere* **2008**, *73*, 461−469.

(16) Tan, X. L.; et al. Sorption of Pb(II) on Na-rectorite: Effects of pH, ionic strength, temperature, soil humic acid and fulvic acid. *Colloid Surf. A-Physicochem. Eng. Asp* **2008**, *328*, 8−14.

(17) Tonkin, J. W.; Balistrieri, L. S.; Murray, J. W. Modeling sorption of divalent metal cations on hydrous manganese oxide using the diffuse double layer model. *Appl. Geochem.* **2004**, *19*, 29−53.

(18) Xu, X. W.; Wang, X. H.; Tang, F.; Zhou, Z. Y. The influencing factors of disposable acetylcholinesterase biosensor for in situ detection of organophosphorus pesticide. *Rare Met. Mater. Eng.* **2006**, *35*, 389−391.

(19) Delage, P.; Cui, Y. J.; Tang, A. M. Clays in radioactive waste disposal. *J. Rock Mech. Geotech. Eng.* **2010**, *2*, 111−123.

(20) Grambow, B. Geological disposal of radioactive waste in clay. *Elements* **2016**, *12*, 239−245.

(21) Landais, P. Advances in geochemical research for the underground disposal of high-level, long-lived radioactive waste in a clay formation. *J. Geochem. Explor.* **2006**, *88*, 32−36.

(22) Bradbury, M. H.; Baeyens, B. Sorption modelling on Illite Part I: Titration measurements and the sorption of Ni, Co, Eu and Sn. *Geochim. Cosmochim. Acta* **2009**, *73*, 990−1003.

(23) Dähn, R.; Baeyens, B.; Bradbury, M. H. Investigation of the different binding edge sites for Zn on montmorillonite using P-EXAFS - The strong/weak site concept in the 2SPNE SC/CE sorption model. *Geochim. Cosmochim. Acta* **2011**, *75*, 5154−5168.

(24) Marques Fernandes, M.; Baeyens, B. Cation exchange and surface complexation of lead on montmorillonite and Illite including competitive adsorption effects. *Appl. Geochem.* **2019**, *100*, 190−202.

(25) Grambow, B.; Fattahi, M.; Montavon, G.; Moisan, C.; Giffaut, E. Sorption of Cs, Ni, Pb, Eu(III), Am(III), Cm, Ac(III), Tc(IV), Th, Zr, and U(VI) on MX80 bentonite: an experimental approach to assess model uncertainty. *Radiochim. Acta* **2006**, *94*, 627−636.

(26) Gu, X. Y.; Evans, L. J.; Barabash, S. J. Modeling the adsorption of Cd (II), Cu (II), Ni (II), Pb (II) and Zn (II) onto montmorillonite. *Geochim. Cosmochim. Acta* **2010**, *74*, 5718−5728.

(27) Akafia, M. M.; Reich, T. J.; Koretsky, C. M. Assessing Cd, Co, Cu, Ni, and Pb sorption on montmorillonite using surface complexation models. *Appl. Geochem.* **2011**, *26*, S154−S157.

(28) Bradbury, M. H.; Baeyens, B. A mechanistic description of Ni and Zn sorption on Na-montmorillonite. Part II: modeling. *J. Contam. Hydrol.* **1997**, *27*, 223−248.

(29) Fletcher, P.; Sposito, G. The chemical modeling of clay/electrolyte interactions for montmorillonite. *Clay Miner.* **1989**, *24*, 375−391.

(30) Tournassat, C.; Grangeon, S.; Leroy, P.; Giffaut, E. Modeling specific pH dependent sorption of divalent metals on montmorillonite surfaces. A review of pitfalls, recent achievements and current challenges. *Am. J. Sci.* **2013**, *313*, 395−451.

(31) Wanner, H.; Albinsson, Y.; Karnland, O.; Wieland, E.; Charlet, L.; Wersin, P. The acid/base chemistry of montmorillonite. *Radiochim. Acta* **1994**, *66-67*, 157−162.

(32) Akpomie, K. G.; Dawodu, F. A.; Adebowale, K. O. Mechanism on the sorption of heavy metals from binary-solution by a low cost montmorillonite and its desorption potential. *Alexandria Eng. J.* **2015**, *54*, 757−767.

(33) Lothenbach, B.; Furrer, G.; Schulin, R. Immobilization of heavy metals by polynuclear aluminium and montmorillonite compounds. *Environ. Sci. Technol.* **1997**, *31*, 1452−1462.

(34) Missana, T.; Alonso, U.; Garcıa-Gutiérrez, M. Experimental study and modelling of selenite sorption onto Illite and smectite clays. *J. Colloid Interface Sci.* **2009**, *334*, 132−138.

(35) Yu, S.; et al. Interaction mechanism of radionickel on Na-montmorillonite: Influences of pH, electrolyte cations, humic acid and temperature. *Chem. Eng. J.* **2016**, *302*, 77−85.

(36) Du, H.; et al. Competitive adsorption of Pb and Cd on bacteria−montmorillonite composite. *Environ. Pollut.* **2016**, *218*, 168−175.

(37) Freitas, E.D.; Carmo, A.C.R.; Almeida Neto, A.F.; Vieira, M.G.A. Binary adsorption of silver and copper on Verde-lodo bentonite: Kinetic and equilibrium study. *Appl. Clay Sci.* **2017**, *137*, 69−76.

(38) Sheikhhosseini, A.; Shirvani, M.; Shariatmadari, H. Competitive sorption of nickel, cadmium, zinc and copper on palygorskite and sepiolite silicate clay minerals. *Geoderma* **2013**, *192*, 249−253.

https://doi.org/10.1021/acsearthspacechem.1c00323
ACS Earth Space Chem. 2022, 6, 144−159

(39) Soltermann, D.; Marques Fernandes, M.; Baeyens, B.; Miehe-Brendle, J.; Dahn, R. Competitive Fe (II)−Zn (II) uptake on a synthetic montmorillonite. *Environ. Sci. Technol.* **2014**, *48*, 190−198.
(40) Vibhawari, B.; Pandey, N. D. Single and competitive sorption of heavy metal ions (Cd2+ & Cu2+) on a clayey soil. *E-J. Chem.* **2010**, *7*, S27−S34.
(41) Bradbury, M. H.; Baeyens, B. Experimental measurements and modeling of sorption competition on montmorillonite. *Geochim. Cosmochim. Acta* **2005**, *69*, 4187−4197.
(42) Flora, S. J. S.; Flora, G.; Saxena, G. Chapter 4 - Environmental occurrence, health effects and management of lead poisoning. *Lead* **2006**, 158−228.
(43) Yadava, K. P.; Tyagi, B. S.; Singh, V. N. Effect of temperature on the removal of lead(II) by adsorption on China clay and wollastonite. *J. Chem. Technol. Biotechnol.* **1991**, *51*, 47−60.
(44) Vardhan, K. H.; Kumar, P. S.; Panda, R. C. A review on heavy metal pollution, toxicity and remedial measures: Current trends and future perspectives. *J. Mol. Liq.* **2019**, *290*, 111197.
(45) Tournassat, C.; Davis, J. A.; Chiaberge, C.; Grangeon, S.; Bourg, I. C. Modeling the acid−base properties of montmorillonite edge surfaces. *Environ. Sci. Technol.* **2016**, *50*, 13436−13445.
(46) Tournassat, C.; Tinnacher, R. M.; Grangeon, S.; Davis, J. A. Modeling uranium(VI) adsorption onto montmorillonite under varying carbonate concentrations: A surface complexation model accounting for the spillover effect on surface potential. *Geochim. Cosmochim. Acta* **2018**, *220*, 291−308.
(47) Drits, V. A.; Zviagina, B. B. Trans-vacant and cis-vacant 2:1 layer silicates: structural features, identification, and occurrence. *Clays Clay Miner.* **2009**, *57*, 405−415.
(48) Tsipursky, S. I.; Drits, V. A. The distribution of octahedral cations in the 2:1 layers of dioctahedral smectites studied by oblique-texture electron diffraction. *Clay Miner.* **1984**, *19*, 177−193.
(49) Bourg, I. C.; Sposito, G.; Bourg, A. C. M. Modeling the acid-base surface chemistry of montmorillonite. *J. Colloid Interface Sci.* **2007**, *312*, 297−310.
(50) Chang, F. R. C.; Sposito, G. The electrical double layer of a disked-shaped clay mineral particle: effect of particle size. *J. Colloid Interface Sci.* **1994**, *163*, 19−27.
(51) Pecini, E. M.; Avena, M. J. Measuring the Isoelectric Point of the Edges of Clay Mineral Particles: The Case of Montmorillonite. *Langmuir* **2013**, *29*, 14926−14934.
(52) Zarzycki, P.; Thomas, F. Theoretical study of the acid-base properties of the montmorillonite/electrolyte interface: Influence of the surface heterogeneity and ionic strength on the potentiometric titration curves. *J. Colloid Interface Sci.* **2006**, *302*, 547−559.
(53) Zhang, C.; Liu, X.; Tinnacher, R. M.; Tournassat, C. Mechanistic understanding of uranyl ion complexation on montmorillonite edges: A combined first-principles molecular dynamics-surface complexation modeling approach. *Environ. Sci. Technol.* **2018**, *52*, 8501−8509.
(54) Liu, X.; et al. Acidity of edge surface sites of montmorillonite and kaolinite. *Geochim. Cosmochim. Acta* **2013**, *117*, 180−190.
(55) Liu, X.; Cheng, J.; Sprik, M.; Lu, X.; Wang, R. Surface acidity of 2:1-type dioctahedral clay minerals from first principles molecular dynamics simulations. *Geochim. Cosmochim. Acta* **2014**, *140*, 410−417.
(56) Liu, X.; Cheng, J.; Sprik, M.; Lu, X.; Wang, R. Interfacial structures and acidity of edge surfaces of ferruginous smectites. *Geochim. Cosmochim. Acta* **2015**, *168*, 293−301.
(57) Bickmore, B. R.; Bosbach, D.; Hochella, M. F. J.; Charlet, L.; Rufe, E. In situ atomic force microscopy study of hectorite and nontronite dissolution: implications for phyllosilicate edge surface structures and dissolution mechanisms. *Am. Mineral.* **2001**, *86*, 411−423.
(58) Churakov, S. V. Ab initio study of sorption on pyrophyllite: Structure and acidity of the edge sites. *J. Phys. Chem. B* **2006**, *110*, 4135−4146.
(59) Newton, A. G.; Sposito, G. Molecular dynamics simulations of pyrophyllite edge surfaces: structure, surface energies, and solvent accessibility. *Clays Clay Miner.* **2015**, *63*, 277−289.
(60) Kraevsky, S. V.; et al. Identification of montmorillonite particle edge orientations by atomic-force microscopy. *Appl. Clay Sci.* **2020**, *186*, 105442.
(61) Suzuki, S.; Sato, H.; Ishidera, T.; Fujii, N. Study on anisotropy of effective diffusion coefficient and activation energy for deuterated water in compacted sodium bentonite. *J. Contam. Hydrol.* **2004**, *68*, 23−37.
(62) Tachi, Y.; Yotsuji, K.; Suyama, T.; Ochs, M. Integrated sorption and diffusion model for bentonite. Part 2: porewater chemistry, sorption and diffusion modeling in compacted systems. *J. Nucl. Sci. Technol.* **2014**, *51*, 1191−11204.
(63) Koch, C. Determination of core structure periodicity and point defect density along dislocations, PhD Thesis, Arizona State University, USA, 2002.
(64) Nadeau, P. H. The physical dimensions of fundamental clay particles. *Clay Miner.* **1985**, *20*, 499.
(65) Parkhurst, D. L., Appelo, C. A. J. Description of input and examples for PHREEQC version 3—A computer program for speciation, batch-reaction, one-dimensional transport, and inverse geochemical calculations: *U.S. Geological Survey Techniques and Methods*, book 6, chap. A43, 2013. Available only at http://pubs.usgs.gov/tm/06/a43/.
(66) Giffaut, E.; et al. Andra thermodynamic database for performance assessment: ThermoChimie. *Appl. Geochem.* **2014**, *49*, 225−236.
(67) Orucoglu, E.; Tournassat, C.; Robinet, J.-C.; Madé, B.; Lundy, M. From experimental variability to the sorption related retention parameters necessary for performance assessment models for nuclear waste disposal systems: The example of Pb adsorption on clay minerals. *Appl. Clay Sci.* **2018**, *163*, 20−32.
(68) Iijima, K.; Tomura, T.; Shoji, Y. Reversibility and modeling of adsorption behavior of cesium ions on colloidal montmorillonite particles. *Appl. Clay Sci.* **2010**, *49*, 262−268.
(69) Gaines, G. L. J.; Thomas, H. C. Adsorption studies on clay minerals. II. A formulation of the thermodynamics of exchange adsorption. *J. Chem. Phys.* **1953**, *21*, 714−718.
(70) Tournassat, C.; et al. Cation exchange selectivity coefficient values on smectite and mixed-layer Illite/smectite minerals. *Soil Sci. Soc. Am. J.* **2009**, *73*, 928−942.
(71) Bradbury, M. H.; Baeyens, B. Modelling the sorption of Mn(II), Co(II), Ni(II), Zn(II), Cd(II), Eu(III), Am(III), Sn(IV), Th(IV), Np(V) and U(VI) on montmorillonite: Linear free energy relationships and estimates of surface binding constants for some selected heavy metals and actinides. *Geochim. Cosmochim. Acta* **2005**, *69*, 875−892.
(72) Churakov, S. V.; Dähn, R. Zinc Adsorption on Clays Inferred from Atomistic Simulations and EXAFS Spectroscopy. *Environ. Sci. Technol.* **2012**, *46*, 5713−5719.
(73) Arai, Y. Effects of dissolved calcium on arsenate sorption at the kaolinite water interface. *Soil Sci.* **2010**, *175*, 207−213.
(74) Hao, W.; et al. The impact of ionic strength on the proton reactivity of clay minerals. *Chem. Geol.* **2019**, *529*, 119294.
(75) Song, X.; Wang, Y.; Cai, J. Sorption of Th(IV) from aqueous solution to GMZ bentonite: effect of pH, ionic strength, fulvic acid and electrolyte ions. *J. Radioanal. Nucl. Chem.* **2013**, *295*, 991−1000.
(76) Liu, X.; Lu, X.; Cheng, J.; Sprik, M.; Wang, R. Temperature dependence of interfacial structures and acidity of clay edge surfaces. *Geochim. Cosmochim. Acta* **2015**, *160*, 91−99.
(77) Baeyens, B., Bradbury, M. H. *A quantitative mechanistic description of Ni, Zn and Ca sorption on Na-montmorillonite. Part I: Physico-chemical characterisation and titration measurements*; Paul Scherrer Institut (PSI), Villigen, 1995.
(78) Duc, M.; Gaboriaud, F.; Thomas, F. Sensitivity of the acid-base properties of clays to the methods of preparation and measurement: 2. Evidence from continuous potentiometric titrations. *J. Colloid Interface Sci.* **2005**, *289*, 148−156.

https://doi.org/10.1021/acsearthspacechem.1c00323
ACS Earth Space Chem. 2022, 6, 144−159

(79) Le Forestier, L.; Muller, F.; Villieras, F.; Pelletier, M. Textural and hydration properties of a synthetic montmorillonite compared with a natural Na-exchanged clay analogue. *Appl. Clay Sci.* **2010**, *48*, 18−25.
(80) Schlegel, M. L.; Manceau, A. Evidence for the nucleation and epitaxial growth of Zn phyllosilicate on montmorillonite. *Geochim. Cosmochim. Acta* **2006**, *70*, 901−917.
(81) Tournassat, C.; Vinsot, A.; Gaucher, E. C.; Altmann, S. Chapter 3 - Chemical conditions in clay-rocks. *Natural and Engineered Clay Barriers* **2015**, *6*, 71−100.
(82) Claret, F.; et al. Natural iodine in a clay formation: Implications for iodine fate in geological disposals. *Geochim. Cosmochim. Acta* **2010**, *74*, 16−29.
(83) Grangeon, S.; et al. The influence of natural trace element distribution on the mobility of radionuclides. The exemple of nickel in a clay-rock. *Appl. Geochem.* **2015**, *52*, 155−173.

https://doi.org/10.1021/acsearthspacechem.1c00323
ACS Earth Space Chem. 2022, 6, 144−159